Alterations of white matter abnormalities in Parkinson's disease: a machine learning approach

long qian
Peking University
chaoyong xiao
Nanjing Brain Hospital Affiliated Nanjing Medical University
Sidong Liu
Macquarie University
zaixu cui
University of Pennsylvania Perelman School of Medicine
xiao hu (283353886@qq.com)
Nanjing Brain Hospital https://orcid.org/0000-0002-4187-7461
weiguo liu
Nanjing Brain Hospital Affiliated Nanjing Medical University

Research Article

Keywords: Parkinson's disease, diffusion tensor imaging, machine learning, linear support vector machine

Posted Date: April 21st, 2021

DOI: https://doi.org/10.21203/rs.3.rs-314254/v1

Abstract

The inter-tract/region dependencies of white-matter in Parkinson's disease are usually ignored by standard statistical tests. Moreover, it remains unclear whether the disruption of white-matter tracts/regions suffices to identify Parkinson's disease patients from healthy controls. A machine learning approach was applied to capture the interdependencies between white-matter tracts/regions and to differentiate PD patients from healthy controls. First, the mean regional white-matter profiles, including white-matter volume, fractional anisotropy, mean diffusivity, axial diffusivity, and radial diffusivity, were extracted as features in Parkinson's disease patients (N = 78) and in healthy controls (N = 91). Then, the feature selection and classification were performed using *t*-test and linear support vector machine, respectively. Last, the relationships between clinical variables and regional magnetic resonance indices were estimated. Our results showed the combined features (white-matter volume, fractional anisotropy, mean diffusivity, axial diffusivity, and radial diffusivity) had the best performance with an accuracy of 75.15% and area under curve of 0.8171, respectively. The most discriminative white-matter features were centered on the association fibers, commissural fibers, projection fibers, and striatal fibers. The discriminative regions of right anterior limb of internal capsule had positive association trends with the Unified Parkinson Disease Rating Scale III score; while the genu of corpus callosum and right retrolenticular part of internal capsule had positively association trends with the Hamilton Depression Rating Scale score. Our finding showed the multivariate machine learning approach is a promising tool to detect abnormal white-matter tracts/regions in Parkinson's disease, and provides us a multidimensional means for neuroimaging classification.

Introduction

Parkinson's disease (PD) is the second most common neurodegenerative disorder in the world, affecting 2-3% of the population over the age of 65 (Poewe, Seppi et al. 2017). Although the precise mechanism underlying the pathophysiology of PD remains unknown, increasing evidences have suggested that pathophysiology of PD was associated with white matter (WM) abnormalities involving a number of brain WM pathways (Juttukonda, Franco et al. 2019, Hu, Qian et al. 2020).

Machine learning (ML) approaches can model multiple variables at the same time, thus being able to discover complicated distribution patterns of the data (Belic, Bobic et al. 2019). Compared with conventional univariate analysis, the advantages of using multivariate ML analysis in neuroimaging data include: 1) enabling the investigation of implicit relationships between different variables, 2) producing an aggregated prediction for individual subject based on the variables collectively. Previous studies have highlighted the importance of shifting neuroimaging analysis from univariate analysis methods to multivariate approaches (Jollans, Boyle et al. 2019, Khosla, Jamison et al. 2019). Moreover, the discriminate patterns discovered using multivariate approaches are independent on *P* values, which may increase false positive rates (Type I error) (Jimenez, Angeles-Valdez et al. 2019), and should be carefully considered in standard test methods (Eklund, Nichols et al. 2016).

Recently, there has been an increasing interest in diffusion tensor imaging (DTI) in PD which implies that the PD pathogenesis might be underlaid by disruptions in WM microstructures (Schulz, Pagano et al. 2018, Juttukonda, Franco et al. 2019). A few previous applications of ML has been proposed in the domain of PD using DTI. Specifically, Haller et al. found that the spatial distribution of abnormal WM regions detected using ML of fractional anisotropy (FA) overlaps substantially with univariate analysis, while the data sample is small and only FA map is applied (Haller, Badoud et al. 2012). Cherubini et al. and Gu et al. demonstrated that the ML approach could help classify PD patients with distinct subtypes or from HC (Cherubini, Morelli et al. 2014, Cherubini, Nistico et al. 2014); however, the detected abnormal spatial patterns were also dependent on conventional univariate statistical test. Du et al. and Liu et al. also applied the ML to distinguish the PD patients from HC using multimodal magnetic resonance imaging (MRI), while only part of brain regions were employed in their classification framework (Liu, Du et al. 2016, Du, Lewis et al. 2017).

On the basis of the above literatures, we hypothesized that: 1) the altered brain patterns across multiple WM regions could be captured in PD patients using multivariate approaches; 2) WM abnormalities could be used to predict PD patients.

Materials And Methods

Study participants and assessment

The Medical Research Ethical Committee of Nanjing Brain Hospital approved the study. In addition, written informed consent was obtained from all the subjects. 78 individuals (39 males) with idiopathic PD and 91 HC (40 males) were recruited. All the participants were right-handed Chinese. In addition, all PD patients fulfilled the UK Parkinson's Disease Society Brain Bank criteria for idiopathic PD (Gibb and Lees 1988). Clinical estimations and MRI scans were performed to exclude acute primary neurological illness, physical illness, and other major psychiatric diseases. The dopamine dosing was stable for at least 4 weeks before and during the study. For PD patients, all neurologic and psychometric evaluations were conducted when patients were in the "on" state, i.e. without showing typical motor symptoms. Motor severity was assessed by the Hoehn and Yahr (H&Y) staging scale and Unified Parkinson's Disease Rating Scale motor part III (UPDRS III). All participants completed the Mini-Mental State Examination (MMSE) and the 17-item Hamilton Depression Rating Scale (HDRS). The image data acquisition was accordance with previous study (Hu, Qian et al. 2020).

Image Processing and feature extraction

With regard to the T1w image, a standard brain segmentation pipeline was performed using DPABI (Yan, Wang et al. 2016), which integrated the SPM12 toolbox (http://www.fil.ion.ucl.ac.uk/spm/). Then, the modulated WMV map was generated for each individual subject (Li, Liu et al. 2020). DTI data analysis was performed using the diffusion image analysis toolbox PANDA (Cui, Zhong et al. 2013). Thereafter, the WMV and diffusion metrics (FA, MD, AD, RD) of the 50 core WM regions defined in ICBM template

were extracted for each subject (Li, Liu et al. 2020). Thus, a matrix of 169 subjects x 50 features was obtained for each WM index.

FS and Classification

In current study, we utilized the two-sample *t*-test (*P* threshold from 0 to 1 with a 0.01 interval) as the FS method (Cui, Xia et al. 2016, Tian, Qian et al. 2020). In addition, a nested leave-one-out cross-validation (LOOCV) strategy was applied in our classification framework **(Figure 1)**, where the selection of optimal feature subsets and evaluation of classification performance were performed in the inner loop and outer loop, respectively (Wee, Yap et al. 2011, Wee, Yap et al. 2012). Furthermore, we applied LSVM to make classification in both the inner and outer LOOCV (Guyon, Weston et al. 2002, Rakotomamonjy 2003). The implementation of LSVM was based on LIBSVM toolbox for Matlab (http://www.csie.ntu.edu.tw/~cjlin/libsvm) (Chang and Lin 2011), and the penalty factor *C* was set at the default value (*C* = 1) (Cui, Xia et al. 2016). For each testing subject, the classification score could be estimated from the LSVM, and the participant with a positive score or negative score was considered as HC or PD, respectively.

Evaluation of the Classification Framework

A total of six indices were estimated to evaluate the classification performance of distinct WM indices-based methods, including AUC (area under the receiver operating characteristic (ROC) curve), accuracy, sensitivity, specificity, positive predictive valve (PPV), and negative predictive value (NPV). In addition, to test whether the AUC and accuracy were significantly higher than values by chance, and whether the classification performance of combined features (WMV, FA, MD, AD, RD) performed better than the single WM index, a permutation test with 1000 times was performed. To control for the error of multiple comparisons among all the six magnetic resonance (MR) indices and each paired comparison, a false-discovery rate (FDR) method was applied.

Discriminative Features

With the utilization of ML approach, the determination of abnormal brain regions was totally different with univariate analysis such as *t*-test. In current study, the most discriminative regions were discovered in the process of cross-validation. Specifically, the FS procedure would be performed once for each outer LOOCV fold after the selection of the optimal *P* threshold. This would result in slightly different selected features for each time. Several studies indicated that the discriminative features referred to the features which selected on all folds of the outer LOOCV (Qian, Zheng et al. 2018, Tian, Qian et al. 2020). Further, the classification contribution of each feature was estimated by averaging the absolute weight across all outer LOOCV folds. The higher discriminative weight, the greater contribution of the corresponding feature (Dai, Yan et al. 2012, Cui, Xia et al. 2016).

Results

Demographic, clinical and test data

To test the group differences in age, education level and neuropsychological scores, the data were analyzed using two-sample *t* test. The gender data were additionally analyzed using χ2 test. Our results demonstrated that no significant differences were found among two groups based on age, gender, years of education and MMSE (all $P > 0.05$). As expected, it showed significant differences between PD and HC in HDRS values, indicating that PD patients experienced significantly more depression symptoms than HC ($P < 0.05$) (**Table 1**).

Classification performance

A total of six kinds of classification framework using single or combined WM indices were evaluated in current study. The classification performance of our results was summarized and demonstrated in **Table 2** and **Figure 2**. Specifically, the combined WMV, FA, MD, AD and RD features- based classification framework could accurately discriminated PD from HC with an AUC of 0.8171. The accuracy, sensitivity, specificity, PPV and NPV were 75.15%, 74.36%, 75.82%, 72.50%, and 77.53%, respectively. Except for WMV and FA, the remaining four WM indices- based approach was demonstrated significantly higher accuracy rate and AUC values than chance ($P < 0.05$). The permutation test indicated that the classification performance of the combined features was significantly higher compared with the WMV, FA or RD index (Combined vs. WMV: $P_{accuracy} = 0.021$, $P_{AUC} = 0.036$; Combined vs. FA: $P_{accuracy} = 0.020$, $P_{AUC} = 0.039$; Combined vs. RD: $P_{accuracy} = 0.042$, $P_{AUC} = 0.047$). Further, we observed that the discrimination capacity of combined features was slightly higher than MD or AD feature (Combined vs. MD: $P_{accuracy} = 0.642$, $P_{AUC} = 0.736$; Combined vs. AD: $P_{accuracy} = 0.724$, $P_{AUC} = 0.697$).

Discriminative WM Features

There were 42 discriminative WM features for the LSVM classifier, which included 6 WMVs, 8 FAs, 10 MDs, 15 ADs, and 3 RDs **(Table 3 and Figure 3)**. Specifically, the 6 WMV features were derived from 3 left WM regions, the external capsule, cingulum, and fornix (cres)/stria terminalis; 3 right WM regions, the tapetum, uncinated fasciculus, and superior longitudinal fasciculus. The 8 regions for the FA feature were derived from 1 bilateral WM regions: the inferior fronto-occipital fasciculus; 2 left WM regions, the uncinate fasciculus, and superior longitudinal fasciculus; 4 right WM regions, the hippocampus part of the cingulum, posterior thalamic radiation, superior fronto-occipital fasciculus, and retrolenticular part of internal capsule. The 10 regions for the MD feature were 3 bilateral WM regions: the inferior fronto-occipital fasciculus, anterior limb of internal capsule, and superior corona radiate; 1 left WM regions, the superior longitudinal fasciculus; 2 right WM regions, the hippocampus part of the cingulum, and retrolenticular part of internal capsule; and 1 middle WM regions, the splenium of corpus callosum. The 15 regions for the AD feature were 2 bilateral WM regions: the inferior fronto-occipital fasciculus, and anterior limb of internal capsule; 3 left WM regions, the superior longitudinal fasciculus, superior corona radiate, and posterior corona radiate; 5 right WM regions, the hippocampus part of the cingulum, posterior limb of internal capsule, retrolenticular part of internal capsule, fornix (cres)/stria terminalis , and

cingulum; and 3 middle WM regions, the genu of corpus callosum, body of corpus callosum, and splenium of corpus callosum. The 3 regions for the RD feature were 1 left WM regions, the superior longitudinal fasciculus; 1 right WM regions, the superior corona radiate; and 1 middle WM regions, the splenium of corpus callosum.

Relationship between discriminative features and clinical variables

The relationships between clinical variables (UPDRS III and HDRS scores) and regional MR indices were estimated. Our results demonstrated that there was no significant correlation in current study ($P < 0.05$), while we observed the association trends in three brain regions ($0.05 < P < 0.1$). Specifically, the discriminative regions of right anterior limb of internal capsule (R = 0.190, $P = 0.096$) had positive association trends with UPDRS III score; while the genu of corpus callosum (R = 0.196, $P = 0.085$) and right retrolenticular part of internal capsule (R = 0.220, $P = 0.053$) were found positively association trends with HDRS score **(Figure 4)**.

Discussion

The current study demonstrated that the aberrant brain patterns in PD could be detected using a multivariate ML approach, and the aberrant WM regions were primarily focused on the association fibers, commissural fibers, projection fibers, and striatal fibers. Second, PD and HC could be well differentiated using WM features and the combined features (WMV, FA, MD, AD, and RD) had the higher classification performance than single feature. Moreover, the discriminative regions of right anterior limb of internal capsule had positive association trends with the UPDRS III score; while the genu of corpus callosum and right retrolenticular part of internal capsule had positively association trends with the HDRS score.

The most discriminative WM connections/regions: The association fibers

As the top discriminative weight in our study, the inferior fronto-occipital fasciculus has the greater contribution of the corresponding feature. The abnormal of inferior fronto-occipital fasciculus was also reported in many previous studies (Zarkali, McColgan et al. 2020) (Wang, Jiang et al. 2016). The inferior fronto-occipital fasciculus, as an important component of the anatomical substrates, involved in peripheral vision and the visual spatial processing (Schmahmann, Smith et al. 2008). Low visual performance showed WM changes within the inferior fronto-occipital fasciculus (Zarkali, McColgan et al. 2020) might account for freezing of gait in PD (Wang, Jiang et al. 2016). As part of the association fibers, the disruption of the uncinate fasciculus tract and superior longitudinal fasciculus integrity is also reported in freezing of gait in PD patients (Pietracupa, Suppa et al. 2018, Tan, Keong et al. 2019). Meanwhile, the axonal damage in the superior longitudinal fasciculus were associated in cognitive impairment in PD (Duncan, Firbank et al. 2016).

Anatomically, the fornix and cingulum comprise the efferent and afferent major fibers of the hippocampus, which are responsible for cognitive deficits in PD (Kamagata, Motoi et al. 2012). Similarly,

abnormalities in the WM fibers that connect the prefrontal cortex to various brain regions, especially the limbic systems, can also cause emotional disturbance in PD patients (Li, Liu et al. 2020).

The inferior longitudinal fasciculus has multiple functions (Herbet, Zemmoura et al. 2018), it has been reported that disruptions of the inferior longitudinal fibers are associated with cognitive impairment, mood disorders, color discrimination deficits, visual hallucinations, freezing of gait, and tremor-dominant motor symptoms in PD patients(Duncan, Firbank et al. 2016, Haghshomar, Dolatshahi et al. 2018, Pietracupa, Suppa et al. 2018, Yuki, Yoshioka et al. 2020).

The most discriminative WM connections/regions: The commissural fibers

Corpus callosum is the largest WM bundle in the human brain (Catani, Howard et al. 2002), can assess the deterioration of inter-hemispheric connectivity. Since it transmits cognitive, sensory and motor information across the hemispheres, and deficits in this area could affect complex motor tasks, such as freezing of gait (Fling, Dale et al. 2016), and cognitive impairment (Bledsoe, Stebbins et al. 2018) in PD patients. The neurodegeneration of corpus callosum in PD may reflect its role in motor, cognitive and emotion features(Dillon, Gonenc et al. 2018), which is in accordance with our finding that the deficits of genu of corpus callosum had positive association trends with HDRS score.

The most discriminative WM connections/regions: The projection fibers

Thalamic fibers have been shown to be involved in the function of the basal ganglia-thalamo-cortical loop, which also affects movement and perception (Shine, Matar et al. 2013). The corona radiata is a dense WM structure that carries almost all of its neural connections from and to the cerebral cortex, as well as to the motor tracts (Guimaraes, Campos et al. 2018). Fiber tracts passing through the internal capsule connect cerebral hemispheres with subcortical structures, brainstem, and spinal cord (Emos and Agarwal 2020). As an important part of the motor circle, damage of the internal capsule may result in clinically symptomatic motor and sensory deficits (Schmahmann, Smith et al. 2008). Previous studies reported that freezing of gait in PD patients showed more pronounced WM abnormalities than HC in the areas of internal capsule, thalamic radiation, and corona radiata (Wang, Jiang et al. 2016, Pietracupa, Suppa et al. 2018, Bharti, Suppa et al. 2019). The anterior limb of internal capsule, where the projection fibers pass from the prefrontal cortex, rostral cingulate area and supplementary motor area, then down to the thalamus, hypothalamus and basis pontis (Schmahmann, Smith et al. 2008), contains fiber tracts that travel transversely between the caudate nucleus and the putamen (Emos and Agarwal 2020). Its deficits related to freezing of gait in PD patients (Pietracupa, Suppa et al. 2018), which accordance with the deficits in the region had positive association trends with UPDRS III score in our study, though not statistically significant. Freezing of gait subtype PD patients or the UPDRS III score was evaluated on the “off” state in PD patients, and there may be a significant correlation in a large data. The retrolenticular segment of the internal capsule contains fibers of the optic radiation which connect the lateral geniculate nucleus to calcarine fissure (Emos and Agarwal 2020). The finding that retrolenticular part of internal capsule was positively correlated with HDRS score was not reported in previous studies, but the abnormal structure and dysfunction of calcarine fissure was found in major depression patients (Chen, Kendrick et

al. 2017) and depressed PD patients (Zhu, Song et al. 2016). We speculated that the abnormal pathway in this “visual region” might indicate sensation and perceptions impairment in patients with depression or altered cognitive functions, such as the ability to pay attention, which may further modulate the mood regulation processes (Zhu, Song et al. 2016).

The most discriminative WM connections/regions: The striatal fibers

Although these corticostriatal pathways allow different regions of the basal ganglia to be involved in motor control, emotion, and cognition , its role in PD may focus on motor control (Wang, Jiang et al. 2016, Pietracupa, Suppa et al. 2018, Bharti, Suppa et al. 2019).

The current study still has a few limitations. First, the executive deficits, and other dysfunctions were not completely assessed in the patients, and it is essential to collect and analyze such data in future studies. Second, due to inter-subject brain differences and scanner variability, it is important to validate the results with a larger sample size and multicenter imaging dataset.

Conclusions

Overall, in the present study, our finding indicated that the multivariate ML approach is a promising choice for detecting abnormal WM tracts/regions in PD, and provides us a multidimensional means for neuroimaging research and classification.

Declarations

Acknowledgments
The authors wish to thank all the participants.

Author Contributions

Author contributions included conception and study design (LQ and XH), data collection or acquisition (CX, XH and WL), statistical analysis (QL and XH), interpretation of results (LQ and XH), drafting the manuscript work or revising it critically for important intellectual content (LQ, XH, SL, ZC and WL) and approval of final version to be published and agreement to be accountable for the integrity and accuracy of all aspects of the work (All authors).

Funding

This work was supported by the National Natural Science Foundation of China (81571348, 81701671), National key research and development plan (2016YFC1306600, 2017YFC1310300, 2017YFC1310302), and Science and Technology Program of Jiangsu Province (BE2019611).

Ethical approval

Ethical approval all procedures performed in studies involving human participants were in accordance with the ethical standards of the institutional and/or national research committee and with the 1964 Helsinki declaration and its later amendments or comparable ethical standards.

Conflict of interest

The authors reported no biomedical financial interests or potential conflict of interest.

Informed consent

Informed consent was obtained from all individual participants included in the study.

References

Belic, M., V. Bobic, M. Badza, N. Solaja, M. Duric-Jovicic and V. S. Kostic (2019). "Artificial intelligence for assisting diagnostics and assessment of Parkinson's disease-A review." Clin Neurol Neurosurg **184**: 105442.

Bharti, K., A. Suppa, S. Pietracupa, N. Upadhyay, C. Gianni, G. Leodori, F. Di Biasio, N. Modugno, N. Petsas, G. Grillea, A. Zampogna, A. Berardelli and P. Pantano (2019). "Abnormal Cerebellar Connectivity Patterns in Patients with Parkinson's Disease and Freezing of Gait." Cerebellum **18**(3): 298-308.

Bledsoe, I. O., G. T. Stebbins, D. Merkitch and J. G. Goldman (2018). "White matter abnormalities in the corpus callosum with cognitive impairment in Parkinson disease." Neurology **91**(24): e2244-e2255.

Catani, M., R. J. Howard, S. Pajevic and D. K. Jones (2002). "Virtual in vivo interactive dissection of white matter fasciculi in the human brain." Neuroimage **17**(1): 77-94.

Chang, C.-C. and C.-J. Lin (2011). "LIBSVM: A library for support vector machines." ACM transactions on intelligent systems and technology (TIST) **2**(3): 27.

Chen, T., K. M. Kendrick, J. Wang, M. Wu, K. Li, X. Huang, Y. Luo, S. Lui, J. A. Sweeney and Q. Gong (2017). "Anomalous single-subject based morphological cortical networks in drug-naive, first-episode major depressive disorder." Hum Brain Mapp **38**(5): 2482-2494.

Cherubini, A., M. Morelli, R. Nistico, M. Salsone, G. Arabia, R. Vasta, A. Augimeri, M. E. Caligiuri and A. Quattrone (2014). "Magnetic resonance support vector machine discriminates between Parkinson disease and progressive supranuclear palsy." Mov Disord **29**(2): 266-269.

Cherubini, A., R. Nistico, F. Novellino, M. Salsone, S. Nigro, G. Donzuso and A. Quattrone (2014). "Magnetic resonance support vector machine discriminates essential tremor with rest tremor from tremor-dominant Parkinson disease." Mov Disord **29**(9): 1216-1219.

Cui, Z., Z. Xia, M. Su, H. Shu and G. Gong (2016). "Disrupted white matter connectivity underlying developmental dyslexia: A machine learning approach." Hum Brain Mapp **37**(4): 1443-1458.

Cui, Z., S. Zhong, P. Xu, Y. He and G. Gong (2013). "PANDA: a pipeline toolbox for analyzing brain diffusion images." Front Hum Neurosci **7**: 42.

Dai, Z., C. Yan, Z. Wang, J. Wang, M. Xia, K. Li and Y. He (2012). "Discriminative analysis of early Alzheimer's disease using multi-modal imaging and multi-level characterization with multi-classifier (M3)." Neuroimage **59**(3): 2187-2195.

Dillon, D. G., A. Gonenc, E. Belleau and D. A. Pizzagalli (2018). "Depression is associated with dimensional and categorical effects on white matter pathways." Depress Anxiety **35**(5): 440-447.

Du, G., M. M. Lewis, S. Kanekar, N. W. Sterling, L. He, L. Kong, R. Li and X. Huang (2017). "Combined Diffusion Tensor Imaging and Apparent Transverse Relaxation Rate Differentiate Parkinson Disease and Atypical Parkinsonism." AJNR Am J Neuroradiol **38**(5): 966-972.

Duncan, G. W., M. J. Firbank, A. J. Yarnall, T. K. Khoo, D. J. Brooks, R. A. Barker, D. J. Burn and J. T. O'Brien (2016). "Gray and white matter imaging: A biomarker for cognitive impairment in early Parkinson's disease?" Mov Disord **31**(1): 103-110.

Eklund, A., T. E. Nichols and H. Knutsson (2016). "Cluster failure: Why fMRI inferences for spatial extent have inflated false-positive rates." Proc Natl Acad Sci U S A **113**(28): 7900-7905.

Emos, M. C. and S. Agarwal (2020). Neuroanatomy, Internal Capsule. StatPearls. Treasure Island (FL).

Fling, B. W., M. L. Dale, C. Curtze, K. Smulders, J. G. Nutt and F. B. Horak (2016). "Associations between mobility, cognition and callosal integrity in people with parkinsonism." Neuroimage Clin **11**: 415-422.

Gibb, W. R. and A. J. Lees (1988). "The relevance of the Lewy body to the pathogenesis of idiopathic Parkinson's disease." J Neurol Neurosurg Psychiatry **51**(6): 745-752.

Guimaraes, R. P., B. M. Campos, T. J. de Rezende, L. Piovesana, P. C. Azevedo, A. C. Amato-Filho, F. Cendes and A. D'Abreu (2018). "Is Diffusion Tensor Imaging a Good Biomarker for Early Parkinson's Disease?" Front Neurol **9**: 626.

Guyon, I., J. Weston, S. Barnhill and V. Vapnik (2002). "Gene selection for cancer classification using support vector machines." Machine learning **46**(1-3): 389-422.

Haghshomar, M., M. Dolatshahi, F. Ghazi Sherbaf, H. Sanjari Moghaddam, M. Shirin Shandiz and M. H. Aarabi (2018). "Disruption of Inferior Longitudinal Fasciculus Microstructure in Parkinson's Disease: A Systematic Review of Diffusion Tensor Imaging Studies." Front Neurol **9**: 598.

Haller, S., S. Badoud, D. Nguyen, V. Garibotto, K. O. Lovblad and P. R. Burkhard (2012). "Individual detection of patients with Parkinson disease using support vector machine analysis of diffusion tensor imaging data: initial results." AJNR Am J Neuroradiol **33**(11): 2123-2128.

Herbet, G., I. Zemmoura and H. Duffau (2018). "Functional Anatomy of the Inferior Longitudinal Fasciculus: From Historical Reports to Current Hypotheses." Front Neuroanat **12**: 77.

Hu, X., L. Qian, Y. Zhang, Y. Xu, L. Zheng, Y. Liu, X. Zhang, Y. Zhang and W. Liu (2020). "Topological changes in white matter connectivity network in patients with Parkinson's disease and depression." Brain Imaging Behav.

Jimenez, S., D. Angeles-Valdez, V. Villicana, E. Reyes-Zamorano, R. Alcala-Lozano, J. J. Gonzalez-Olvera and E. A. Garza-Villarreal (2019). "Identifying cognitive deficits in cocaine dependence using standard tests and machine learning." Prog Neuropsychopharmacol Biol Psychiatry: 109709.

Jollans, L., R. Boyle, E. Artiges, T. Banaschewski, S. Desrivieres, A. Grigis, J. L. Martinot, T. Paus, M. N. Smolka, H. Walter, G. Schumann, H. Garavan and R. Whelan (2019). "Quantifying performance of machine learning methods for neuroimaging data." Neuroimage **199**: 351-365.

Juttukonda, M. R., G. Franco, D. J. Englot, Y. C. Lin, K. J. Petersen, P. Trujillo, P. Hedera, B. A. Landman, H. Kang, M. J. Donahue, P. E. Konrad, B. M. Dawant and D. O. Claassen (2019). "White matter differences between essential tremor and Parkinson disease." Neurology **92**(1): e30-e39.

Kamagata, K., Y. Motoi, O. Abe, K. Shimoji, M. Hori, A. Nakanishi, T. Sano, R. Kuwatsuru, S. Aoki and N. Hattori (2012). "White matter alteration of the cingulum in Parkinson disease with and without dementia: evaluation by diffusion tensor tract-specific analysis." AJNR Am J Neuroradiol **33**(5): 890-895.

Khosla, M., K. Jamison, G. H. Ngo, A. Kuceyeski and M. R. Sabuncu (2019). "Machine learning in resting-state fMRI analysis." Magn Reson Imaging.

Li, Z., W. Liu, C. Xiao, X. Wang, X. Zhang, M. Yu, X. Hu and L. Qian (2020). "Abnormal white matter microstructures in Parkinson's disease and comorbid depression: A whole-brain diffusion tensor imaging study." Neurosci Lett **735**: 135238.

Liu, H., G. Du, L. Zhang, M. M. Lewis, X. Wang, T. Yao, R. Li and X. Huang (2016). "Folded concave penalized learning in identifying multimodal MRI marker for Parkinson's disease." J Neurosci Methods **268**: 1-6.

Pietracupa, S., A. Suppa, N. Upadhyay, C. Gianni, G. Grillea, G. Leodori, N. Modugno, F. Di Biasio, A. Zampogna, C. Colonnese, A. Berardelli and P. Pantano (2018). "Freezing of gait in Parkinson's disease: gray and white matter abnormalities." J Neurol **265**(1): 52-62.

Poewe, W., K. Seppi, C. M. Tanner, G. M. Halliday, P. Brundin, J. Volkmann, A. E. Schrag and A. E. Lang (2017). "Parkinson disease." Nat Rev Dis Primers **3**: 17013.

Qian, L., L. Zheng, Y. Shang, Y. Zhang and Y. Zhang (2018). "Intrinsic frequency specific brain networks for identification of MCI individuals using resting-state fMRI." Neurosci Lett **664**: 7-14.

Rakotomamonjy, A. (2003). "Variable selection using svm based criteria." The Journal of Machine Learning Research **3**: 1357-1370.

Schmahmann, J. D., E. E. Smith, F. S. Eichler and C. M. Filley (2008). "Cerebral white matter: neuroanatomy, clinical neurology, and neurobehavioral correlates." Ann N Y Acad Sci **1142**: 266-309.

Schulz, J., G. Pagano, J. A. Fernandez Bonfante, H. Wilson and M. Politis (2018). "Nucleus basalis of Meynert degeneration precedes and predicts cognitive impairment in Parkinson's disease." Brain **141**(5): 1501-1516.

Shine, J. M., E. Matar, P. B. Ward, S. J. Bolitho, M. Gilat, M. Pearson, S. L. Naismith and S. J. Lewis (2013). "Exploring the cortical and subcortical functional magnetic resonance imaging changes associated with freezing in Parkinson's disease." Brain **136**(Pt 4): 1204-1215.

Tan, S. Y. Z., N. C. H. Keong, R. M. P. Selvan, H. Li, L. Q. R. Ooi, E. K. Tan and L. L. Chan (2019). "Periventricular White Matter Abnormalities on Diffusion Tensor Imaging of Postural Instability Gait Disorder Parkinsonism." AJNR Am J Neuroradiol **40**(4): 609-613.

Tian, Z. Y., L. Qian, L. Fang, X. H. Peng, X. H. Zhu, M. Wu, W. Z. Wang, W. H. Zhang, B. Q. Zhu, M. Wan, X. Hu and J. Shao (2020). "Frequency-Specific Changes of Resting Brain Activity in Parkinson's Disease: A Machine Learning Approach." Neuroscience **436**: 170-183.

Wang, M., S. Jiang, Y. Yuan, L. Zhang, J. Ding, J. Wang, J. Zhang, K. Zhang and J. Wang (2016). "Alterations of functional and structural connectivity of freezing of gait in Parkinson's disease." J Neurol **263**(8): 1583-1592.

Wee, C. Y., P. T. Yap, K. Denny, J. N. Browndyke, G. G. Potter, K. A. Welsh-Bohmer, L. Wang and D. Shen (2012). "Resting-state multi-spectrum functional connectivity networks for identification of MCI patients." PLoS One **7**(5): e37828.

Wee, C. Y., P. T. Yap, W. Li, K. Denny, J. N. Browndyke, G. G. Potter, K. A. Welsh-Bohmer, L. Wang and D. Shen (2011). "Enriched white matter connectivity networks for accurate identification of MCI patients." Neuroimage **54**(3): 1812-1822.

Yan, C. G., X. D. Wang, X. N. Zuo and Y. F. Zang (2016). "DPABI: Data Processing & Analysis for (Resting-State) Brain Imaging." Neuroinformatics **14**(3): 339-351.

Yuki, N., A. Yoshioka, R. Mizuhara and T. Kimura (2020). "Visual hallucinations and inferior longitudinal fasciculus in Parkinson's disease." Brain Behav: e01883.

Zarkali, A., P. McColgan, L. A. Leyland, A. J. Lees, G. Rees and R. S. Weil (2020). "Fiber-specific white matter reductions in Parkinson hallucinations and visual dysfunction." Neurology **94**(14): e1525-e1538.

Zhu, Y., X. Song, M. Xu, X. Hu, E. Li, J. Liu, Y. Yuan, J. H. Gao and W. Liu (2016). "Impaired interhemispheric synchrony in Parkinson's disease with depression." Sci Rep **6**: 27477.

Tables

Table1. Demographic and neuropsychological characteristics of all subjects

	HC(n=91)	PD(n=78)	*P* value
	Mean±SD	Mean±SD	
Age(years)	57.67±5.27	58.69±6.83	0.275
Education(years)	10.92±4.52	11.01±3.44	0.886
Gender(M/F)	40/51	39/39	0.432#
MMSE	28.85±2.30	28.51±1.54	0.279
HDRS	3.06 ± 3.65	12.86 ± 8.62	0.0001
UPDRS III	NA	26.28±12.79	NA
H&Y	NA	2.43±2.12	NA
PD duration time	NA	5.96±3.70	NA

Values are represented as the mean ± SD. For comparisons of demographics, #*P* value for the gender distribution in the two groups was obtained using a test. Comparisons of neuropsychological scores between the two groups (HC, PD) were analyzed using a two-sample *t* tests. NA-not applicable. F-female; M-male. $P<0.05$ was considered significant.

Table 2. Classification results of the LSVM classifier using a single or combined features (LOOCV)

Feature	AUC	Accuracy	Sensitivity	Specificity	PPV	NPV
WMV	0.5416	0.5207	0.1795	0.8132	0.4516	0.5362
FA	0.5289	0.5444	0.359	0.7033	0.5091	0.5614
MD	0.7677	0.7369	0.7308	0.7473	0.7125	0.764
AD	0.7959	0.7278	0.6923	0.7582	0.7105	0.7417
RD	0.6657	0.6864	0.5641	0.7912	0.6984	0.6792
Combined	0.8171	0.7515	0.7436	0.7582	0.725	0.7753

PPV: positive predictive value; NPV: negative predictive value.

Table 3. The discriminative features of LSVM classifier

Regions	Hemisphere	Metric	ROI	Discriminative weight
Inferior fronto-occipital fasciculus	R	AD	45	0.202
Cingulum (hippocampus part)	R	FA	37	0.174
Cingulum (hippocampus part)	R	AD	37	0.158
Genu of corpus callosum		AD	3	0.136
Uncinate fasciculus	L	FA	48	0.128
Posterior thalamic radiation (include optic radiation)	R	FA	29	0.126
Body Genu of corpus callosum		AD	4	0.121
Superior corona radiata	L	AD	26	0.119
Anterior limb of internal capsule	R	AD	17	0.117
Inferior fronto-occipital fasciculus	R	FA	45	0.116
Inferior fronto-occipital fasciculus	L	AD	46	0.113
Splenium of corpus callosum		AD	5	0.111
Tapetum	R	WMV	49	0.108
Anterior limb of internal capsule	L	AD	18	0.102
External capsule	L	WMV	34	0.1
Superior longitudinal fasciculus	L	AD	42	0.098
Inferior fronto-occipital fasciculus	L	FA	46	0.097
Superior fronto-occipital fasciculus	R	FA	43	0.096
Splenium of corpus callosum		MD	5	0.09
Posterior limb of internal capsule	R	AD	19	0.09
Inferior fronto-occipital fasciculus	R	MD	45	0.087
Uncinate fasciculus	R	WMV	47	0.086
Anterior limb of internal capsule	R	MD	17	0.083
Retrolenticular part of internal capsule	R	FA	21	0.083
Cingulum (cingulated part)	R	AD	35	0.082
Superior longitudinal fasciculus.	L	MD	42	0.082
Cingulum (cingulated part)	L	WMV	36	0.08
Retrolenticular part of internal capsule	R	AD	21	0.079
Cingulum (hippocampus part)	R	MD	37	0.079
Superior longitudinal fasciculus	R	WMV	41	0.078
Superior longitudinal fasciculus	L	FA	42	0.077
Anterior limb of internal capsule	L	MD	18	0.075
Fornix.(cres)./.Stria.terminalis	R	AD	39	0.075
Splenium of corpus callosum		RD	5	0.07
Superior corona radiata	R	MD	25	0.068
Inferior fronto-occipital fasciculus	L	MD	46	0.068
Posterior corona radiata	L	AD	28	0.065
Superior corona radiata	R	RD	25	0.064
Superior corona radiata	L	MD	26	0.064
Retrolenticular part of internal capsule	R	MD	21	0.063
Fornix.(cres)./.Stria.terminalis	L	WMV	40	0.063
Superior longitudinal fasciculus	L	RD	42	0.062

L: left; R: right.

Figures

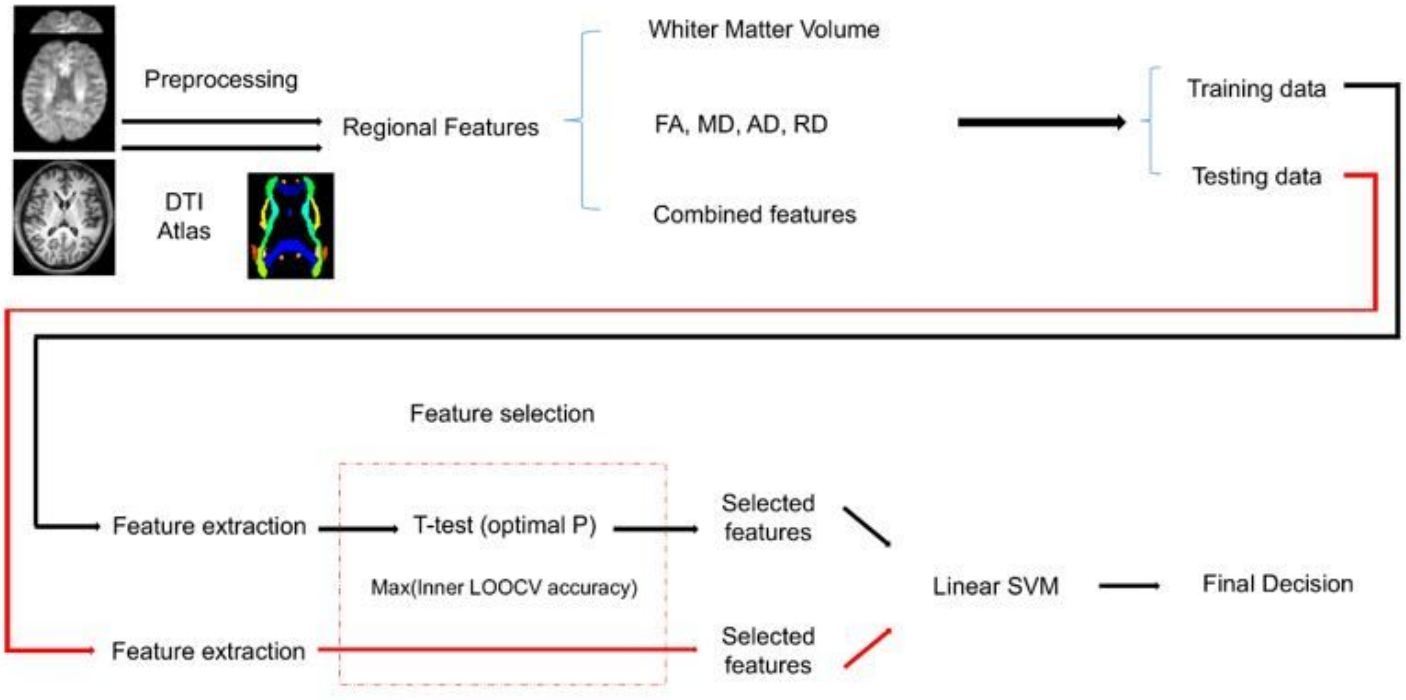

Figure 1

Schematic diagram of the combined WM features- based classification framework. The mean regional WM profiles, including WM volume (WMV), fractional anisotropy (FA), mean diffusivity (MD), axial diffusivity (AD), and radial diffusivity (RD), were extracted as features. Then, the feature selection and classification were performed using the t-test and linear support vector machine (LSVM), respectively. A nested leave one out cross-validation (LOOCV) was applied for feature selection and classifier training.

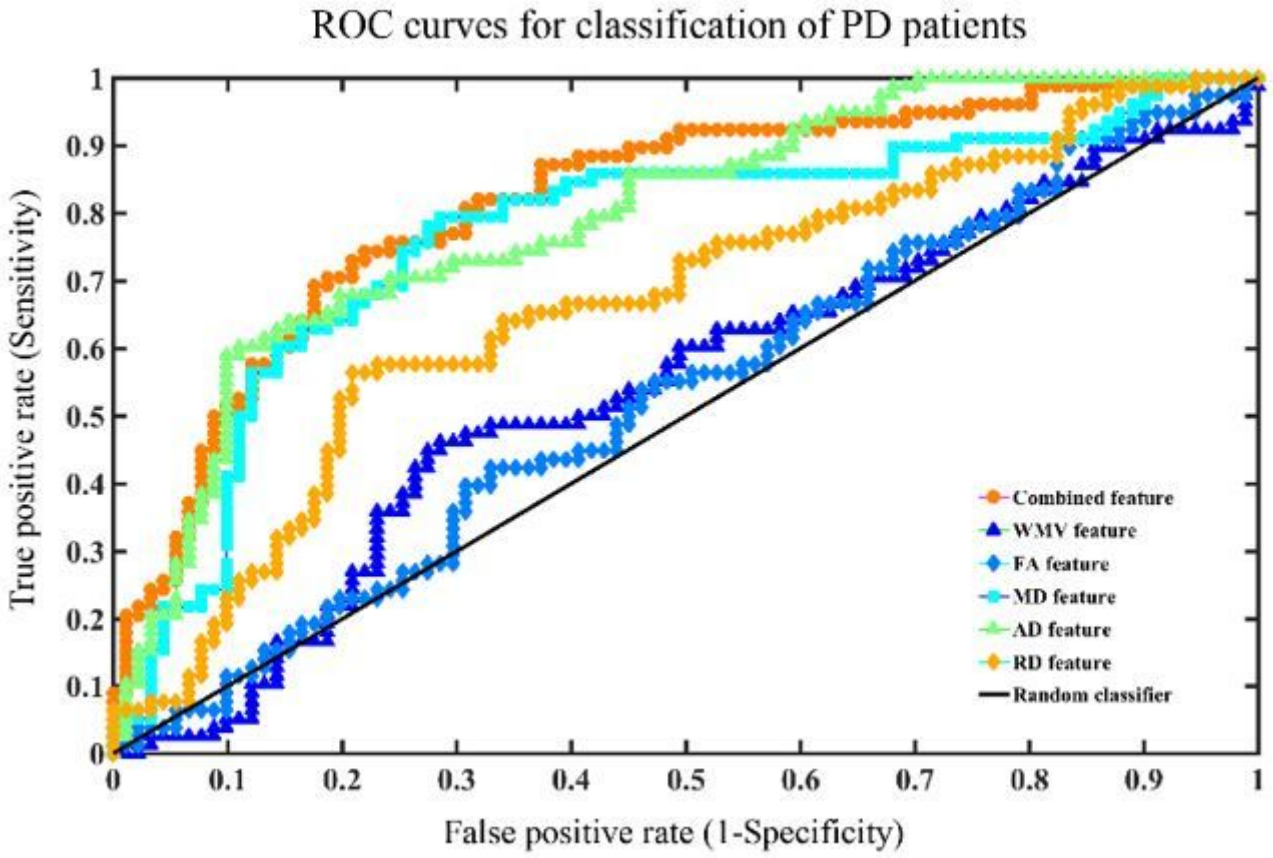

Figure 2

Receiver operating characteristic (ROC) curves for classification of PD patients using single or combined WM features. In current study, a total of six kinds of classification framework using single or combined WM indices were evaluated in current study. The classification performance of our results was summarized in Table 2. The area under ROC (AUC) for the combined features and WMV, FA, MD, AD and RD features were 0.82, 0.54, 0.53, 0.77, 0.80, and 0.67, respectively.

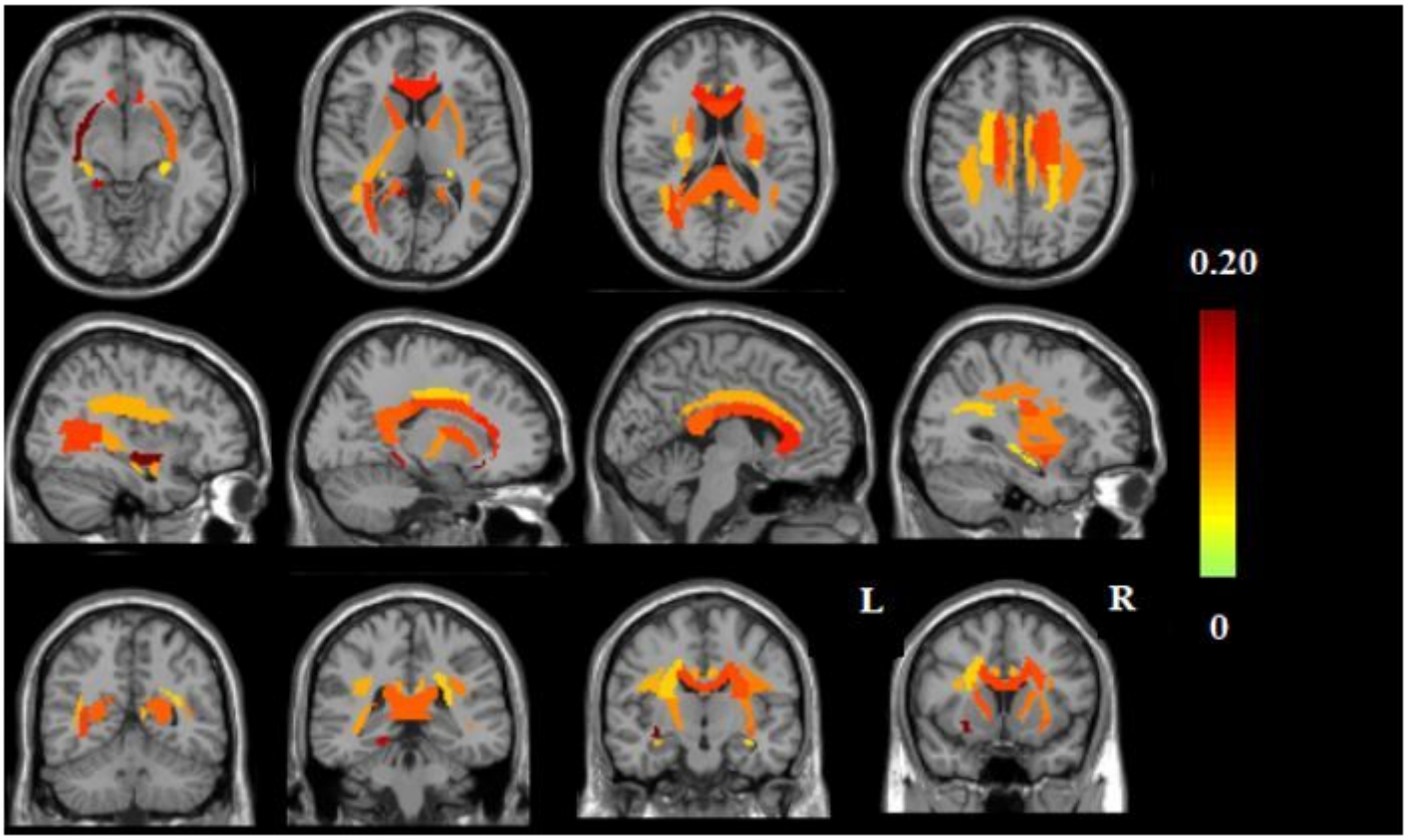

Figure 3

The discriminated regions of interest (ROIs) selected for classification. There were 42 discriminative WM features for the LSVM classifier, which included 6 WMVs, 8 FAs, 10 MDs, 15 ADs, and 3 RDs (Table 3).

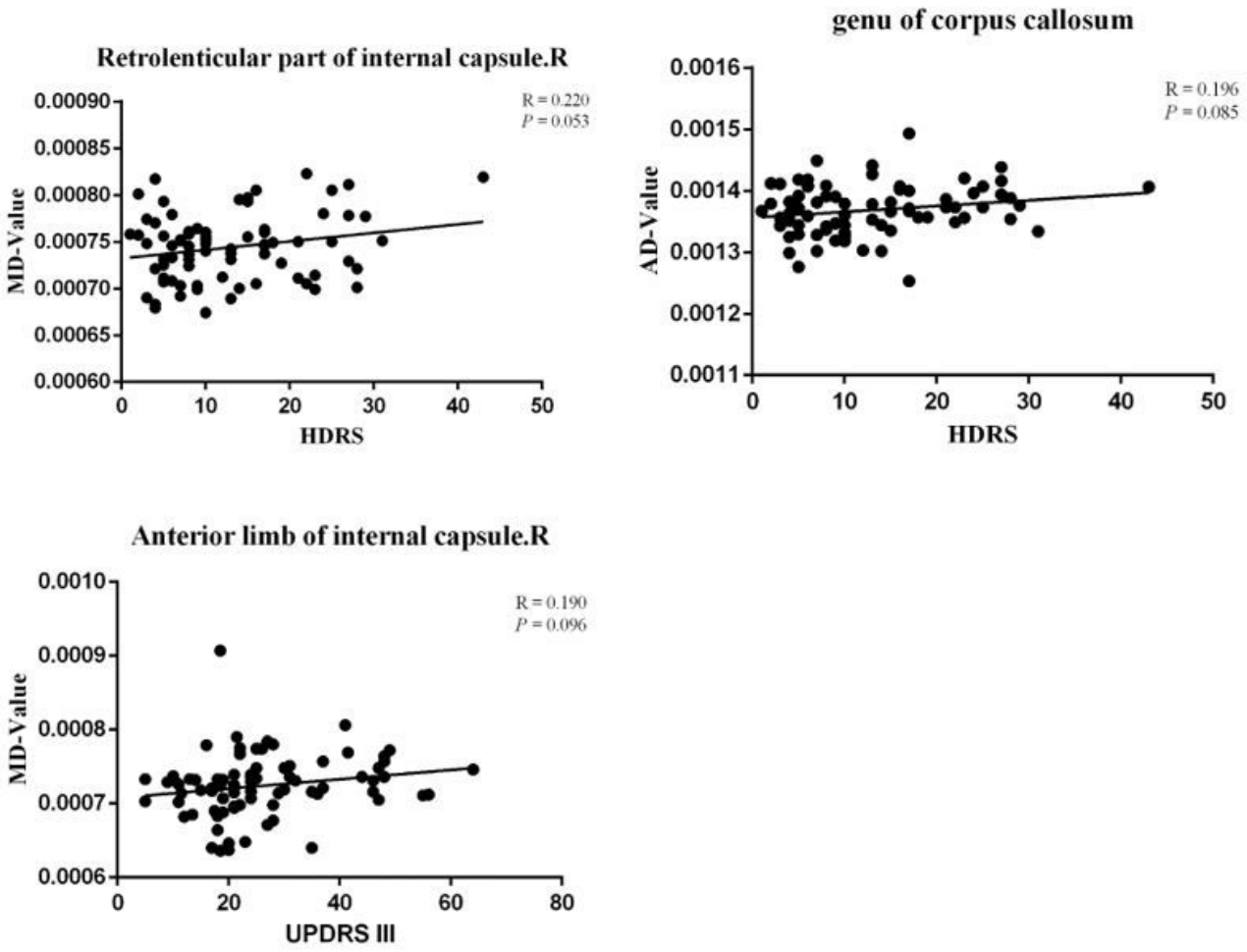

Figure 4

Relationship between the discriminative WM features and clinical variables. We demonstrated that there was no significant correlation in current study ($P < 0.05$), while we observed the association trends in three brain regions ($0.05 < P < 0.1$).

Supplementary Files

This is a list of supplementary files associated with this preprint. Click to download.

- BIBChecklist.docx